Enhancement of NIR-Absorbing Ability of Bis(diarylmethylium)-Type Dicationic Dyes Based on an *Ortho*-Substitution Strategy

Takashi Harimoto,[a] Takanori Suzuki,[a] and Yusuke Ishigaki*[a]

[a] Mr. T. Harimoto, Prof. Dr. T. Suzuki, Prof. Dr. Y, Ishigaki
Department of Chemistry, Faculty of Science
Hokkaido University
N10 W8, North-ward, Sapporo 060-0810, Japan
E-mail: yishigaki@sci.hokudai.ac.jp

Abstract: Electrochromic systems capable of switching near-infrared (NIR) absorption are fascinating from the viewpoint of applications in the materials and life sciences. Although 11,11,12,12-tetraaryl-9,10-anthraquinodimethanes (AQDs) with a folded form undergo one-stage two-electron oxidation to produce twisted dicationic dyes exhibiting NIR absorption, there is a need to establish a design strategy that can enhance the NIR-absorbing abilities of the corresponding dicationic dyes. In this study, we designed and synthesized a series of anthraquinodimethane derivatives with various substituents introduced at the *ortho*-position(s) of the 4-methoxyphenyl group. X-ray and spectroscopic analyses revealed that NIR-absorbing properties can be changed by introduction of the *ortho* substituents. Thus, control of the steric and electronic effects of the *ortho* substituents on the 4-methoxyphenyl groups was demonstrated to be an effective strategy for fine-tuning of the HOMO and LUMO levels for neutral AQDs and twisted dications, respectively, resulting in the modification of electrochemical and spectroscopic properties under an "*ortho*-substitution strategy".

Introduction

Organic dyes such as cyanines,[1–3] squaliums,[4,5] and diimmoniums,[6,7] and organometallic complexes such as nickel dithiolenes[8] and phthalocyanines[9] show a narrow energy gap which has been attributed to a long-range π-conjugation based on the effective delocalization of N/O-based cations and charge-transfer (CT) interactions based on metal ions, respectively. Thus, they are known to exhibit near-infrared (NIR) absorption in the range of 700–2000 nm.[10–12] These dyes are expected to be applied to various optical applications such as security marking,[13,14] lithography,[15] optical filters[16,17] and photovoltaic cells.[18–22] Furthermore, to increase the efficiency of photovoltaic power generation, it would be desirable to make effective use of NIR light in sunlight. Thus, the development of NIR-absorbing materials is of essential importance.[23–25] In addition, since NIR light shows a superior penetration of biological tissues, NIR dyes are also expected to be applied to chemotherapy and imaging of deep tissues in vivo.[26–34]

Electrochromic systems, on the other hand, induce drastic color changes based on the redox interconversion between neutral and charged species.[35,36] Electrochromic systems capable of switching NIR absorption are attractive from the viewpoint of applications for material and life science, and thus several examples have been reported to date.[37–40] Since most of the inorganic systems contain heavy metals, the development of organic-based materials is needed to reduce the environmental impact and improve biocompatibility.

However, since the redox states of organic NIR dyes are generally unstable, the reversible modulation of NIR absorption based on quantitative redox interconversion is still a challenging issue regarding reversibility and durability during their interconversion. Indeed, there is an increasing interest in organic electrochromic systems that enable ON/OFF switching of NIR absorption.[41,42,51,43–50]

We recently reported that 11,11,12,12-tetraaryl-9,10-anthraquinodimethanes (AQDs) **1** with a folded form undergo one-stage two-electron oxidation to produce twisted dications with a planar anthracene skeleton (Scheme 1).[52,53] The HOMO of the dication $\mathbf{1}^{2+}$ is mainly located on the anthracene framework, and the corresponding LUMO is delocalized in two diarylmethylium units. As a result, a NIR absorption band (~800 nm) based on an intramolecular CT interaction from HOMO to LUMO was observed in the dication with 4-methoxyphenyl groups. Therefore, lowering the LUMO level of dicationic dyes is an effective approach for the observation of longer-wavelength absorption in the NIR region.

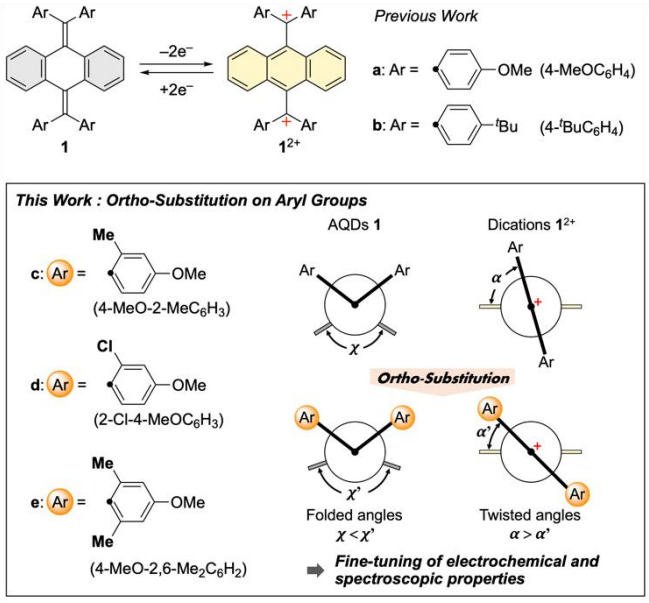

Scheme 1. Redox interconversion of anthraquinodimethane derivatives and molecular designs based on an "*ortho*-substitution strategy''.

Therefore, we aimed to obtain advanced design guidelines to control the wavelength of NIR bands by the introduction of proper substituents to 4-methoxyphenyl groups. In this study, we newly designed and synthesized a series of AQD-based electrochromic systems with *ortho*-substituents on 4-methoxyphenyl groups. X-ray analyses and electrochemical and spectroscopic

measurements of both neutral and cationic species revealed their detailed structural and electronic properties both experimentally and theoretically. As a result, both the electronic and steric effects of the *ortho* substituents were proven to be effective for controlling the CT bands in the NIR region. Notably, not only an electron-withdrawing substituent such as chlorine atom but also an electron-donating substituent such as methyl group can lower the LUMO level of the dication $\mathbf{1}^{2+}$ to exhibit longer-wavelength absorption. Since lowering the LUMO level with electron-withdrawing groups often leads to the undesirable consequence of decreased stability of dicationic dyes, this "*ortho*-substitution strategy", which enables the enhancement of NIR-absorbing abilities by lowering the LUMO levels of the chromophores, is key for constructing reversible NIR electrochromic materials

Results and Discussion

The target compounds **1c** and **1d** with a methyl group and chlorine atom at the *ortho*-position of a 4-methoxyphenyl group, respectively, were obtained in good yields by the Suzuki-Miyaura cross-coupling reaction of tetrabromoanthraquinodimethane **2**[54] with the corresponding aryl boronic acid (Scheme 2). An *ortho*-disubstituted derivative **1e** was synthesized by the Negishi cross-coupling reaction (Scheme 2). Single-crystal X-ray structure analyses revealed that all these derivatives adopt a folded conformation, as in 4-methoxyphenyl derivative **1a** (Figure 1). Notable differences in the structural features of these AQD derivatives were found in **1e** with two *ortho* substituents (Table 1). Thus, the bent angles θ_{exp} between the central plane and diarylethene moieties decrease due to the steric effects in **1e** with two *ortho* substituents (39.04(11)°, 44.39(10)° for **1a**, 36.65(5)° for **1c**, 33.16(14)°, 33.45(14)° for **1d** and 27.04(10)°, 29.79(11)° for **1e**). In particular, **1e** has a unique torsion angle ϕ and folded angle χ [ϕ = 13.05(9)° and 18.24(8)°, χ = 34.85(13)°], which suggests that neutral **1e** has a folded-twisted conformation with smaller *p*-orbital overlap for the exomethylene bonds.

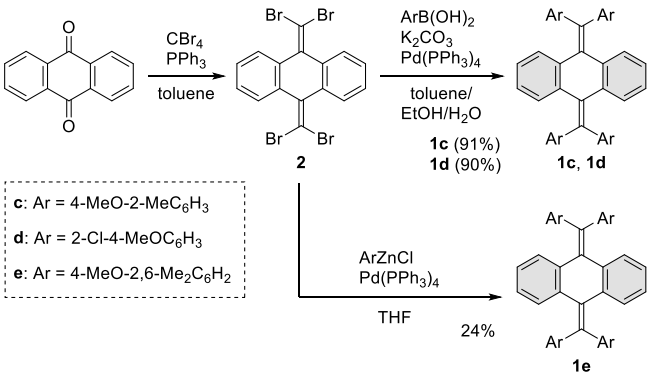

Scheme 2. Preparation of *ortho*-substituted derivatives **1c**–**1e**.

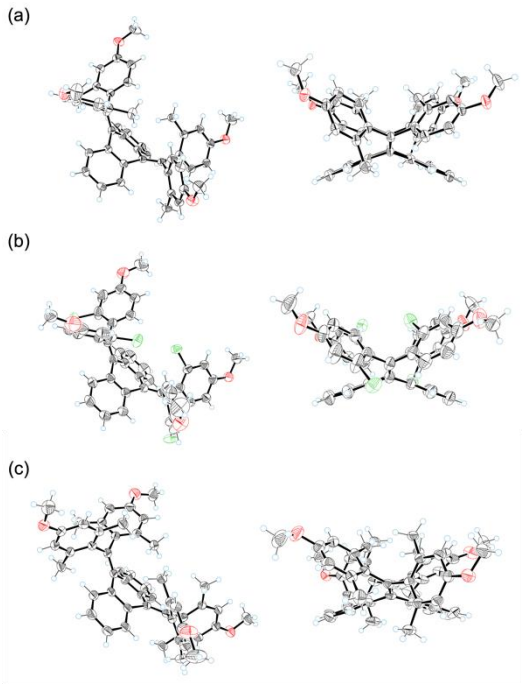

Figure 1. X-ray crystal structures (ORTEP drawings) of (a) **1c**, (b) **1d**, and (c) **1e** determined at 150 K. Thermal ellipsoids are shown at the 50% probability level.

Table 1. Structural parameters determined by X-ray analyses and DFT calculations (CAM-B3LYP/6-31G*). The calculated values are shown in italics.

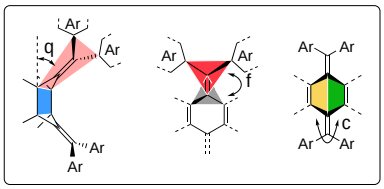

		θ (°)	ϕ (°)	χ (°)
1a	Expt.	44.39(10)	7.32(8)	47.22(12)
		39.04(11)	9.45(9)	-
	Calcd.	*39.11*	*7.236*	*45.13*
		39.11	*7.240*	-
1c	Expt. [a]	36.65(5)	3.72(7)	41.84(16)
	Calcd.	*34.91*	*4.132*	*41.91*
		34.91	*4.126*	-
1d	Expt.	33.16(14)	4.73(11)	38.66(17)
		33.45(14)	7.21(11)	-
	Calcd.	*37.68*	*6.444*	*42.87*
		36.62	*6.630*	-
1e	Expt.	27.04(10)	18.24(8)	34.85(13)
		29.79(11)	13.05(9)	-
	Calcd.	*27.36*	*15.71*	*34.73*
		27.06	*15.87*	-

[a] Centrosymmetric.

To investigate the redox behavior of *ortho*-substituted AQDs **1c**–**1e** in detail, cyclic voltammetry (CV) measurements were performed in CH_2Cl_2 (Figure 2). Cyclic voltammograms of **1c** and **1d** showed two-electron oxidation peaks at +1.06 V and +1.32 V vs. SCE, respectively, for which a two-electron process was confirmed using ferrocene as an external standard. The value of methyl derivative **1c** is similar to that of **1a** (+1.03 V) whereas the higher oxidation potential of **1d** can be accounted for by the introduction of electron-withdrawing chlorine atoms. As a result of changes in their structures, return peaks, at which twisted dications undergo two-electron reduction to give folded neutral species, appeared in the far cathodic region (+0.59 V for $\mathbf{1c}^{2+}$ and +0.87 V for $\mathbf{1d}^{2+}$). Such peak separation is a characteristic feature of dynamic redox (dyrex) systems such as **1a**/$\mathbf{1a}^{2+}$, in which the steady-state concentration of an intermediate radical species is negligible.[55]

The most important finding is that both $\mathbf{1d}^{2+}$ with chlorine atoms and $\mathbf{1c}^{2+}$ with methyl groups exhibit higher reduction potentials than $\mathbf{1a}^{2+}$, proving that electron-donating groups at the *ortho* position can also lower the LUMO of the dication. Actually, the reduction peak corresponding to $\mathbf{1e}^{2+}$ with two methyl groups on each aryl group exhibits a much higher reduction peak at +0.66 V, showing that steric effects of the *ortho*-substituents can lower the LUMO of the dications even if they have electron-donating substituents on the 4-methoxyphenyl group. In contrast to **1c** and **1d** with a large separation of redox peaks, the voltammogram of **1e** showed almost no separation. This would result from the easy oxidation of **1e** with a folded-twisted geometry at +0.78 V. Such a small separation might suggest that there is no significant structural change that accompanies redox interconversion between **1e** and dication $\mathbf{1e}^{2+}$. However, this is not the case, as proven in the next section by isolation and analysis of the X-ray structure of $\mathbf{1e}^{2+}$ salt as well as other dications.

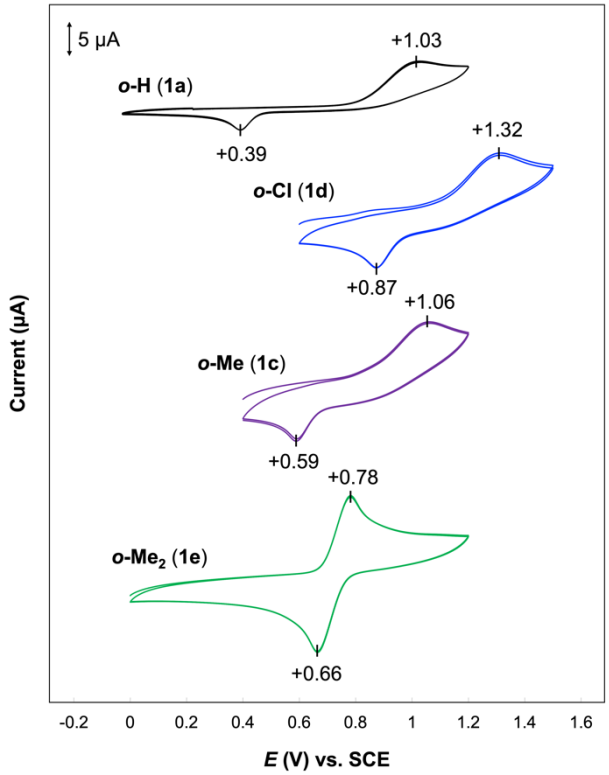

Figure 2. Cyclic voltammograms of neutral donors ***o*-H** (**1a**), ***o*-Cl** (**1d**), ***o*-Me** (**1c**), and ***o*-Me₂** (**1e**) at 297 K in CH_2Cl_2 containing 0.1 M Bu_4NBF_4 as a supporting electrolyte (scan rate 0.1 V s^{-1}, Pt electrodes).

The dicationic salts $\mathbf{1}^{2+}(SbCl_6^-)_2$ were successfully synthesized and isolated quantitatively by treatment of the neutral donor with 2 equivalents of $(4\text{-}BrC_6H_4)_3N^{+\bullet}SbCl_6^-$ (Magic Blue) (Figure 3a). X-ray analysis showed that, in common with dication $\mathbf{1a}^{2+}$, dications $\mathbf{1c}^{2+}$–$\mathbf{1e}^{2+}$ adopt a fully conjugated planar anthracene core (Figure 3b). Notably, the steric repulsion of the *ortho*-substituents leads to a decrease in the average twist angles α_{exp} between the anthracene core and the diarylmethylium moiety (76.7° for $\mathbf{1a}^{2+}$, 67.0° for $\mathbf{1c}^{2+}$, 66.6° for $\mathbf{1d}^{2+}$ and 50.7° for $\mathbf{1e}^{2+}$). Moreover, the torsion angles β_{exp} between the aryl group and methylium moiety increase to avoid steric repulsion between *ortho*-substituents (24.3(3)° for $\mathbf{1a}^{2+}$, 27.5(7)° and 31.6(8)° for $\mathbf{1c}^{2+}$, 30.0(4)° and 38.6(8)° for $\mathbf{1d}^{2+}$ and 43.35(9)° and 43.36(9)° for $\mathbf{1e}^{2+}$). Density functional theory (DFT) calculations[56] at the CAM-B3LYP/6-31G* level showed dihedral angles α and β similar to those observed (Table 2). Treatment of the dications with an excess amount of Zn powder quantitatively regenerated the original neutral AQDs **1**. This result indicates that a reversible redox interconversion proceeds between neutral state **1** and dicationic state $\mathbf{1}^{2+}$, resulting in a dynamic structural change upon electron transfer.

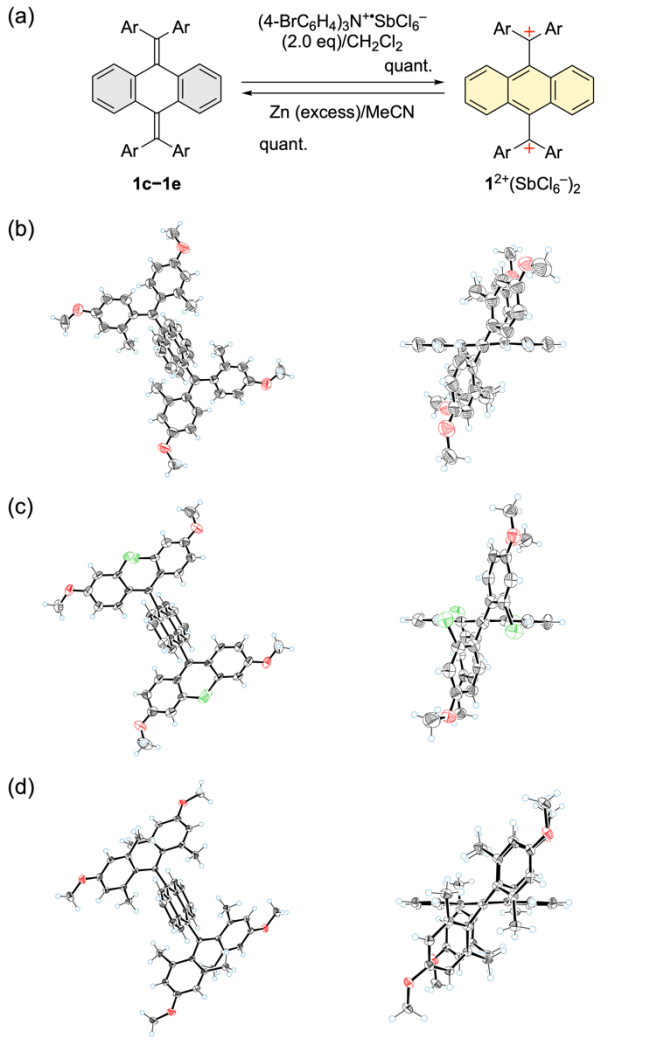

Figure 3. (a) Redox interconversion of *ortho*-substituted derivatives $\mathbf{1c}/\mathbf{1c}^{2+}(SbCl_6^-)_2$, $\mathbf{1d}/\mathbf{1d}^{2+}(SbCl_6^-)_2$, and $\mathbf{1e}/\mathbf{1e}^{2+}(SbCl_6^-)_2$. X-ray crystal structures (ORTEP drawings) of (b) $\mathbf{1c}^{2+}(SbCl_6^-)_2$, (c) $\mathbf{1d}^{2+}(SbCl_6^-)_2$, and (d) $\mathbf{1e}^{2+}(SbCl_6^-)_2$ determined at 150 K. Thermal ellipsoids are shown at the 50% probability level. The counterions are omitted for clarity.

Table 2. Structural parameters determined by X-ray analyses and DFT calculations (CAM-B3LYP/6-31G*). The calculated values are shown in italics.

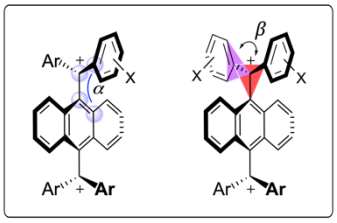

		α_{ave} (°)	β (°)
1a^{2+}	Expt.[a]	76.7	24.3(3)
	Calcd.	*71.69*	*24.87*, *24.88*
1c^{2+}	Expt. [a]	67.0	33.8(5), 34.4(4)
	Calcd.	*64.42*	*30.35*, *35.18*
1d^{2+}	Expt. [a]	66.6	30.0(4), 38.1(4)
	Calcd.	*69.30*	*32.67*, *33.85*
1e^{2+}	Expt. [a]	50.7	43.35(9), 43.36(9)
	Calcd.	*54.89*	*40.95*, *40.96*

[a] Centrosymmetric.

The *ortho*-monosubstituted neutral compounds **1c** and **1d** in CH_2Cl_2 exhibit absorption mainly in the UV region, and no significant difference in absorption properties was observed compared to AQD **1a**. In contrast, *ortho*-disubstituted neutral **1e** shows a more red-shifted absorption band (λ_{max} = 394 nm) into the visible region compared to *ortho*-monosubstituted derivatives **1c** and **1d** (Figure S9). The observed red-shift for **1e** can be explained by the adoption of a folded-twisted conformation which has a higher HOMO and a lower LUMO than the corresponding folded structure, resulting in a decrease in the HOMO-LUMO gap. Elevation of the HOMO level was experimentally demonstrated by CV measurement (*vide supra*).

On the other hand, dication salts **1c**$^{2+}$−**1e**$^{2+}$ in CH_2Cl_2 exhibit strong absorption, mainly in the Vis/NIR region (Figure 4). The red-shift of the strong absorption band in the visible region, which is attributed to the π-π* transition derived from the diarylmethylium chromophore, was observed from λ_{max} (nm) = 532 (**1a**$^{2+}$) to 650 (**1e**$^{2+}$) (Table 2), accompanied by a decrease in the molar absorption coefficient ε ($Lmol^{-1}cm^{-1}$) from 162000 (**1a**$^{2+}$) to 47100 (**1e**$^{2+}$) (Table 2). The significant changes in the values of λ_{max} and **ε** can be explained by perturbation of the frontier orbital level due to the steric effect of the *ortho*-substituents. The steric repulsion between *ortho*-substituents increases the torsion angle β between the aryl group and methylium moiety (Table 1), which weakens the effective delocalization of the positive charge and the oscillator strength of the π-π* transition. The NHOMO-LUMO gap and oscillator strength corresponding to the π-π* transition are reproduced by TD-DFT calculations (Figure S6).

Another striking result is the NIR absorption of **1e**$^{2+}$. The first absorption band in the NIR region is attributed to the intramolecular CT transition from HOMO mainly located on the anthracene core to LUMO delocalized on diarylmethylium units. The CT band was red-shifted from λ_{max} (ε) = 709 nm (8650) for **1a**$^{2+}$ to 855 nm (21100) for **1e**$^{2+}$ (Table 2), which is due to the narrower HOMO-LUMO gap induced by the steric effects of *ortho*-substituents.

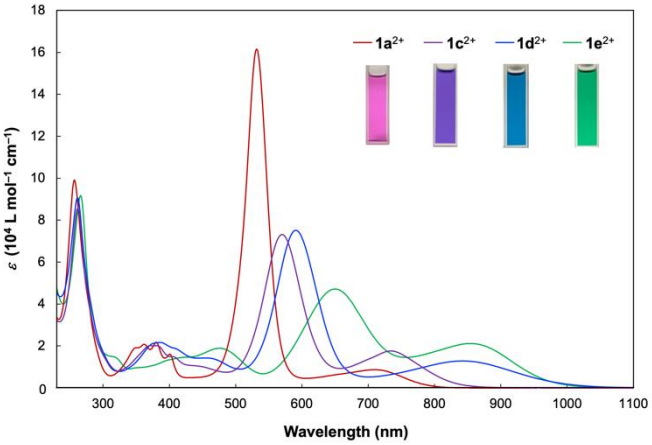

Figure 4. UV/Vis/NIR spectra of **1a**$^{2+}$$(SbCl_6^-)_2$ (red), **1c**$^{2+}$$(SbCl_6^-)_2$ (blue), **1d**$^{2+}$$(SbCl_6^-)_2$ (violet), and **1e**$^{2+}$$(SbCl_6^-)_2$ (green) in CH_2Cl_2.

Table 3. UV/Vis/NIR spectral data of the dication salts in CH_2Cl_2.

	λ_{max} (ε)
1a^{2+}$(SbCl_6^-)_2$	709 nm (8650), 532 nm (162000)
1c^{2+}$(SbCl_6^-)_2$	734 nm (17600], 570 nm (73100)
1d^{2+}$(SbCl_6^-)_2$	843 nm (12800), 591 nm (75100)
1e^{2+}$(SbCl_6^-)_2$	855 nm (21100), 650 nm (47100)

In this way, we could successfully extend the NIR absorption band by lowering the LUMO level without attaching electron-withdrawing substituents to the aryl group. We previously observed that a red-shift of the NIR absorption band extending to 1000 nm could be achieved for another dication **1b**$^{2+}$ with *tert*-butylphenyl groups (Scheme 1), by lowering the LUMO due to the absence of a methoxy group.[48] However, the dication **1b**$^{2+}$ is too moisture-sensitive because it is composed of pure hydrocarbon without electron-donating heteroatoms. Another merit of the use of an *ortho*-substitution strategy is the enhancement of **ε** of the NIR absorption bands. In general, for twisted dications such as **1a**$^{2+}$, the CT transitions are virtually forbidden because the two units of diarylmethylium are attached to the anthracene in an almost orthogonal manner, and the transition intensities are relatively minimal. Thus, the much larger ε in **1e**$^{2+}$ can also be explained by the steric effect, which reduced the twist angle α between the diarylmethylium unit and the anthracene core (Table 1) and increased the overlap of the HOMO-LUMO orbitals, resulting in an increase in the oscillator strength of the CT transitions. As a result, the terminus of the CT band of **1e**$^{2+}$ reaches 1100 nm, and the corresponding ε is approximately 2.4 times greater than that of **1a**$^{2+}$.

To obtain further information regarding the effect of the twist angle α between the diarylmethylium unit and the central anthracene core on the frontier orbital levels, we performed DFT calculations. For example, in the case of **1a**$^{2+}$, we predict that reducing its twist angle α can induce a red-shift and an enhancement of the oscillator strength in the CT band, when optimizations were performed by varying the twist angle $\alpha\angle$C1-C2-C3-C4 in steps of 20° from the initial optimized structure (α = 71.69°) while keeping the four aryl *ipso*-carbons C4, C5, C6, and C7 fixed on the same plane (Figure 5). According to DFT calculations, the HOMO-

LUMO gap becomes narrower as the twist angle α decreases [α = 71.69° (ΔE = 4.27 eV), 51.69° (4.16 eV), 31.69° (4.02 eV), 11.69° (3.86 eV), Figure S7]. In fact, TD-DFT calculations for each of the optimized structures revealed that the CT bands show a constant red-shift as the twist angle α decreases from 71.69° to 11.69°. In addition, it was also demonstrated that the oscillator strength *f* of the first absorption band gradually increases from 0.1681 to 0.4053. Notably, with a decrease in the twist angle α, the average torsion angle β_{ave} increases [α = 71.69° (β_{ave} = 24.88°), 51.69° (26.64°), 31.69° (29.14°), 11.69° (32.33°), Figure S7], leading to a red-shift in the second absorption band and a decrease in the oscillator strength *f* from 1.4114 to 0.5508.

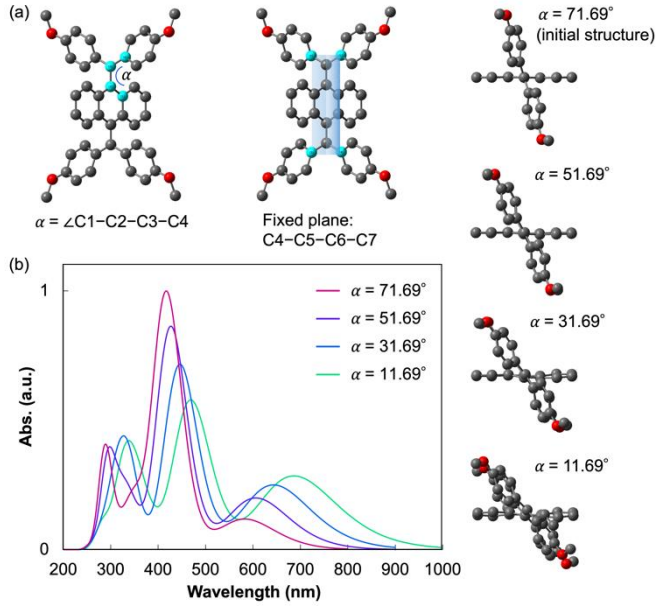

Figure 5. (a) Optimized structures obtained by varying the twist angle α ∠C1-C2-C3-C4 with the fixed plane C4−C5−C6−C7 from the energy-minimized structure (α = 71.69°) for **1a**$^{2+}$. (b) A change in UV/Vis/NIR spectrum simulated by TD-DFT calculations of **1a**$^{2+}$ while varying the twist angle α.

Based on this theoretical result, for *ortho*-disubstituted **1e**$^{2+}$, to confirm whether the experimentally observed red-shift was due to a decrease in the twist angle α, theoretical calculations with varying of the corresponding angle were conducted in the same procedure. As a result, TD-DFT calculations carried out under conditions of varying the twist angle α∠C1-C2-C3-C4 in steps of 10° from the initial optimized structure (α = 54.89°) show a constant blue-shift accompanied by a decrease in the oscillator strength *f* from 0.2840 to 0.1604 (Figure S8). Therefore, the energy levels of frontier orbitals are significantly affected by the twist angles α between the diarylmethylium units and anthracene cores. Thus, modulation of the steric and electronic effects of *ortho*-substituents is an effective strategy that allows a fine-tuned red-shift of both the first and second absorption bands. A similar behavior was also observed for biaryl-type molecules.[57,58]

Finally, constant-current electrochemical oxidation of the *ortho*-monosubstituted electron donor **1c** was monitored by UV/Vis/NIR spectroscopy in CH_2Cl_2 (Figure 6). The colorless solution gradually turned deep violet with several isosbestic points, demonstrating that an intermediate radical species is short-lived in this process, as in other dyrex systems such as **1a**/**1a**$^{2+}$. Regeneration of **1c** accompanied by a color change from deep violet color to nearly colorless was confirmed by reduction of as-prepared **1c**$^{2+}$ when the polarity of the electrodes was reversed (Figure S10). Therefore, by introducing a substituent on the *ortho*-position of 4-methoxyphenyl groups, it is possible to extract an even longer wavelength-shifted NIR absorption upon electrochemical stimulation.

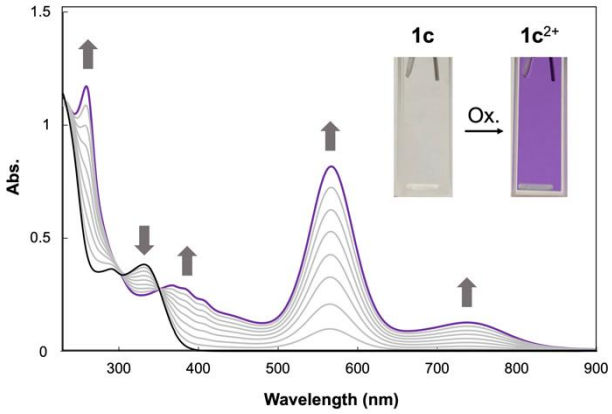

Figure 6. A change in the UV/Vis/NIR spectrum upon constant-current electrochemical oxidation of **1c** (22.1 μM, 30 μA, every 16 min) in CH_2Cl_2 containing 0.05 M Bu_4NBF_4 as a supporting electrolyte.

Conclusion

In summary, we have designed and synthesized a series of AQD derivatives with various substituents at the *ortho*-position of the 4-methoxyphenyl group. Quantitative redox interconversions between neutral *ortho*-substituted AQDs and the corresponding dications were demonstrated on a preparative scale. X-ray crystallographic analyses of these derivatives revealed that the *ortho* substituents have a significant steric effect on both the neutral and dicationic states. Electrochemical measurements suggest that the steric and electronic effects of *ortho* substituents can modify both the redox behavior and potential, especially for *ortho*-disubstituted derivative **1e**/**1e**$^{2+}$. Furthermore, UV/Vis/NIR spectroscopy showed that the two main absorption bands of the dicationic dye can be controlled by adjusting the steric effects of the *ortho* substituents. In particular, the end-absorption of the CT band of **1e**$^{2+}$ reaches 1100 nm, and the corresponding ε is enhanced up to 2.4 times larger than that of **1a**$^{2+}$. The *ortho*-substitution strategy, which allows fine-tuning of the HOMO/LUMO levels, is expected to lead to NIR absorption-switchable redox systems, paving the way for the development of functional organic dyes in materials and life science.

Experimental Section

All reactions were carried out under an argon atmosphere. All commercially available compounds were used without further purification. Dry MeCN was obtained by distillation from CaH_2 prior to use. Column chromatography was performed on silica gel 60N (KANTO KAGAKU, spherical neutral) of particle size 40-50 μm or Wakogel® 60N (neutral) of particle size 38-100 μm. ^{1}H and ^{13}C NMR spectra were recorded on a BRUKER Ascend™ 400 (^{1}H/400 MHz and ^{13}C/100MHz) spectrometer at 296 K unless otherwise indicated. IR spectra were measured on a Shimadzu IRAffinity-1S spectrophotometer using the attenuated total reflection (ATR) mode. Mass spectra were recorded on a JMS-T100GCV spectrometer in FD mode by Dr. Eri Fukushi and Mr. Yusuke Takata (GS-MS & NMR Laboratory, Research Faculty of Agriculture, Hokkaido University). Melting points were measured on a Yamato MP-21 and are

uncorrected. UV/Vis/NIR spectra were recorded on a JASCO V-770 spectrophotometer. Redox potentials (E^{ox} and E^{red}) were measured on a BAS ALS-612EX by cyclic voltammetry in dry CH_2Cl_2 containing 0.1 M Bu_4NBF_4 as a supporting electrolyte. All of the values shown in the text are in *E*/*V* vs. SCE measured at the scan rate of 100 mVs^{-1}. Pt electrodes were used as the working (disk) and counter electrodes. The working electrode was polished using a water suspension of aluminum oxide (0.05 μm) before use. DFT calculations were performed with the Gaussian 16W program package.[56] The geometries of the compounds were optimized by using the CAM-B3LYP method in combination with the 6-31G* basis set unless otherwise indicated.

Preparation of 11,11,12,12-tetrakis(4-methoxy-2-methylphenyl)-9,10-anthraquinodimethane (1c): A mixture of 11,11,12,12-tetrabromo-9,10-anthraquinodimethane[54] (780 mg, 1.50 mmol), 4-methoxy-2-methylphenylboronic acid (1.49 g, 9.00 mmol), K_2CO_3 (1.66 g, 12.0 mmol) and $Pd(PPh_3)_4$ (86.7 mg, 75.0 μmol) in toluene (15 mL), EtOH (1.5 mL), and H_2O (1.5 mL) was stirred at reflux for 14 h. After cooling to 25 ºC, the mixture was diluted with water and extracted with EtOAc five times. The combined organic layers were washed with water and brine, and dried over anhydrous Na_2SO_4. After filtration, the solvent was concentrated under reduced pressure. The crude product was purified by column chromatography on silica gel (hexane/CH_2Cl_2 = 1) to give **1c** (926 mg) as a white solid in 90% yield.
Mp: 259-260 ºC; ^{1}H NMR (400 MHz, $CDCl_3$ at 330 K): δ/ppm 7.35 (4H, brs), 7.10 (4H, brs), 6.70 (12H, m), 3.75 (12H, s), 2.13 (12H, brs); ^{13}C NMR (100 MHz, $CDCl_3$): δ/ppm 158.21, 137.39, 136.00, 133.49, 130.98, 128.56, 126.43, 125.48, 125.06, 115.45, 111.48, 55.06, 21.57; IR (ATR): *v*/cm^{-1} 3065, 3011, 2993, 2953, 2934, 2906, 2831, 1605, 1568, 1496, 1463, 1448, 1416, 1375, 1311, 1288, 1261, 1230, 1173, 1157, 1118, 1098, 1044, 988, 934, 864, 842, 829, 815, 797, 769, 749, 731, 726, 704, 668, 654, 630, 603, 585, 564, 541, 493, 446; LR-MS(FD) m/z (%): 687.38 (5), 686.38 (17), 685.38 (54), 684.37 (M^+, bp), 343.19 (1), 342.69 (4), 342.19 (M^{2+}, 7); HR-MS (FD) Calcd. for $C_{48}H_{44}O_4$: 684.32396; Found: 684.32260; UV/Vis (CH_2Cl_2): λ_{max}/nm (ε/$Lmol^{-1}cm^{-1}$) 332 (17400), 291 (16400).

Preparation of 11,11,12,12-tetrakis(2-chloro-4-methoxyphenyl)-9,10-anthraquinodimethane (1d): A mixture of 11,11,12,12-tetrabromo-9,10-anthraquinodimethane[54] (1.04 mg, 2.00 mmol), 2-chloro-4-methoxyphenylboronic acid (1.79 g, 9.60 mmol), K_2CO_3 (1.77 g, 12.8 mmol) and $Pd(PPh_3)_4$ (116 mg, 100 μmol) in toluene (20 mL), EtOH (2.0 mL), and H_2O (2.0 mL) was stirred at 80 ºC for 20 h. After cooling to 25 ºC, the mixture was diluted with water and extracted with EtOAc five times. The combined organic layers were washed with water and brine, and dried over anhydrous Na_2SO_4. After filtration, the solvent was concentrated under reduced pressure. The crude product was purified by column chromatography on silica gel (hexane/EtOAc = 5) to give **1d** (1.39 g) as a white solid in 91% yield.
Mp: 261-263 ºC; ^{1}H NMR (400 MHz, $CDCl_3$): δ/ppm 8.18 (2H, d, *J* = 8.4 Hz), 7.41-7.28 (4H, m), 7.08 (2H, d, *J* = 7.6 Hz), 7.03 (2H, d, *J* = 2.0 Hz), 6.77 (2H, d, *J* = 7.6 Hz), 6.73 (2H, d, *J* = 2.0 Hz), 6.69 (2H, d, *J* = 8.4 Hz), 3.77 (6H, s), 3.74 (6H, s); ^{13}C NMR (100 MHz, $CDCl_3$): δ/ppm 159.10, 158.93, 139.35, 136.94, 136.44, 134.63, 134.34, 133.41, 132.82, 132.04, 131.45, 130.62, 127.68, 126.57, 125.97, 125.51, 115.09, 114.81, 113.18, 113.03, 55.41, 55.38; IR (ATR): *v*/cm^{-1} 3074, 3005, 2956, 2935, 2905, 2834, 1599, 1555, 1490, 1458, 1437, 1399, 1284, 1256, 1220, 1182, 1039, 976, 949, 894, 882, 873, 854, 845, 833, 810, 794, 766, 732, 719, 685, 655, 626, 610, 594, 573, 559, 483, 457; LR-MS(FD) m/z (%): 771.15 (8), 770.15 (18), 769.15 (26), 768.15 (57), 767.15 (48), 766.15 (bp), 765.15 (36), 764.15 (M^+, 69), 383.08 (7), 382.08 (M^{2+}, 5); HR-MS (FD) Calcd. for $C_{44}H_{32}Cl_4O_4$: 764.10547; Found: 764.10540; UV/Vis (CH_2Cl_2): λ_{max}/nm (ε/$Lmol^{-1}cm^{-1}$) 310 (sh, 17200), 290 (20000).

Preparation of 11,11,12,12-tetrakis(4-methoxy-2,6-dimethylphenyl)-9,10-anthraquinodimethane (1e): To a solution of 2-bromo-5-methoxy-1,3-dimethylbenzene[59] (1.33 g, 6.19 mmol) in dry THF (30 mL) was added *n*BuLi (1.59 M solution in hexane, 3.9 mL, 6.19 mmol) dropwise over 5 min at -78 ºC, and the mixture was stirred for 1 h. To the solution was added dichloro(*N*,*N*,*N*',*N*'-tetramethylethane-1,2-diamine)zinc(II) (suspension in THF, 15 mL, 6.19 mmol) dropwise over 5 min at -78 ºC. The mixture was gradually warmed up to -50 ºC, and stirred for 1 h. To the solution were added 11,11,12,12-tetrabromo-9,10-anthraquinodimethane[54] (535 mg, 1.03 mmol) and $Pd(PPh_3)_4$ (119 mg, 103 μmol), and the mixture was stirred at reflux for 44 h. After cooling to 25 ºC, the mixture was diluted with water and extracted with EtOAc five times. The combined organic layers were washed with water and brine, and dried over anhydrous Na_2SO_4. After filtration, the solvent was concentrated under reduced pressure. The crude product was purified by column chromatography on silica gel (hexane/EtOAc = 7) to give **1e** (181 mg) as a yellow solid in 24% yield.
Mp: 230-231 ºC; ^{1}H NMR (400 MHz, $CDCl_3$): δ/ppm 7.35 (4H, dd, *J* = 3.4, 6.1 Hz), 6.74 (4H, dd, *J* = 3.4, 6.1 Hz), 6.48 (8H, s), 3.75 (12H, s), 2.32 (12H, brs), 1.98 (12H, brs); ^{13}C NMR (100 MHz, $CDCl_3$): δ/ppm 158.05, 140.56, 140.31, 137.53, 137.05, 136.64, 135.22, 127.79, 125.61, 114.91, 112.37, 54.92, 22.96, 22.02; IR (ATR): *v*/cm^{-1} 3051, 3003, 2934, 2917, 2834, 1600, 1569, 1476, 1456, 1437, 1371, 1309, 1273, 1195, 1154, 1138, 1112, 1070, 1064, 1032, 996, 947, 854, 842, 835, 770, 740, 716, 693, 664, 654, 631, 603, 586, 512; LR-MS(FD) m/z (%): 743.46 (6), 742.45 (20), 741.44 (60), 740.44 (M^+, bp); HR-MS (FD) Calcd. for $C_{52}H_{52}O_4$: 740.38656; Found: 740.38881; UV/Vis (CH_2Cl_2): λ_{max}/nm (ε/$Lmol^{-1}cm^{-1}$) 394 (24900).

Preparation of anthracene-9,10-diyl-bis[bis(4-methoxy-2-methylphenyl)methylium] bis(hexachloroantimonate) [$1c^{2+}(SbCl_6^-)_2$]: To a solution of **1c** (119 mg, 174 μmol) in dry CH_2Cl_2 (5.1 mL) was added tris(4-bromophenyl)aminium hexachloroantimonate (283 mg, 347 μmol), and the mixture was stirred at 25 ºC for 30 min. The addition of dry ether led to precipitation of the dication salt. The precipitates were washed with dry ether five times, and collected by filtration to give $\mathbf{1c}^{2+}(SbCl_6^-)_2$ (229 mg) as a dark-violet powder in 97% yield.
Mp: 164-165 ºC; ^{1}H NMR (400 MHz, CD_3CN): δ/ppm 7.62 (4H, dd, *J* =3.3, 6.9 Hz), 7.54 (4H, dd, *J* =3.3, 6.9 Hz), 7.47 (4H, d, *J* = 8.3 Hz), 7.20 (4H, brs), 7.09 (4H, d, *J* = 8.3 Hz), 4.12 (12H, s), 2.04 (12H, brs); ^{13}C NMR (100 MHz, CD_3CN): δ/ppm 190.70, 173.45, 152.46, 146.19, 142.11, 139.15, 132.40, 130.04, 126.62, 122.14, 116.43, 58.32, 22.50; IR (ATR, KBr pellet) : *v*/cm^{-1} 3078, 2978, 2941, 2841, 1603, 1583, 1559, 1522, 1456, 1441, 1423, 1358, 1301, 1266, 1226, 1188, 1174, 1105, 1065, 1031, 997, 944, 927, 858, 818, 767, 730, 562, 513; LR-MS(FD) m/z (%): 685.32 (12), 684.31 ($[M^{2+}+e^-]^+$, 29), 344.16 (2), 343.66 (6), 343.16 (16), 342.66 (56), 342.16 (M^{2+}, bp); HR-MS (FD) Calcd. for $C_{48}H_{44}O_4$: 684.32396; Found: 684.32558; UV/Vis/NIR (CH_2Cl_2): λ_{max}/nm (ε/$Lmol^{-1}cm^{-1}$) 734 (17600), 570 (73100), 262 (85500).

Preparation of anthracene-9,10-diyl-bis[bis(2-chloro-4-methoxyphenyl)methylium] bis(hexachloroantimonate) [$\mathbf{1d}^{2+}(SbCl_6^-)_2$]: To a solution of **1d** (218 mg, 284 μmol) in dry CH_2Cl_2 (5.7 mL) was added tris(4-bromophenyl)aminium hexachloroantimonate (464 mg, 568 μmol), and the mixture was stirred at 25 ºC for 30 min. The addition of dry ether led to precipitation of the dication salt. The precipitates were washed with dry ether five times, and collected by filtration to give $\mathbf{1d}^{2+}(SbCl_6^-)_2$ (397 mg) as a dark-blue powder in 97% yield.
Mp: 193-194 ºC; ^{1}H NMR (400 MHz, CD_3CN): δ/ppm 7.72-7.57 (12H, m), 7.46 (4H, d, *J* = 2.4 Hz), 7.18 (4H, d, *J* = 9.0 Hz), 4.17 (12H, s); ^{13}C NMR (100 MHz, CD_3CN): δ/ppm 187.10, 174.53, 146.72, 145.50, 142.59, 136.24, 133.17, 130.47, 126.75, 122.22, 117.38, 59.34; IR (ATR, KBr pellet) : *v*/cm^{-1} 3102, 2942, 2843, 1596, 1573, 1522, 1437, 1417, 1364, 1306, 1260, 1212, 1180, 1159, 1138, 1041, 1009, 928, 870, 816, 762, 736, 718, 608, 550; LR-MS(FD) m/z (%): 771.16 (6), 770.16 (16), 769.16 (22), 768.16 (50), 767.16 (42), 766.16 (86), 765.16 (32), 764.16 ($[M^{2+}+e^-]^+$, 59), 386.07 (5), 385.58 (9), 385.08 (19), 384.58 (27), 384.08 (58), 383.58 (47), 383.08 (bp), 382.58 (34), 382.08 (M^{2+}, 66); HR-MS (FD) Calcd. for $C_{44}H_{32}Cl_4O_4$: 764.10547; Found: 764.10426; UV/Vis/NIR (CH_2Cl_2): λ_{max}/nm (ε/$Lmol^{-1}cm^{-1}$) 843 (12800), 591 (75100), 385 (21600), 262 (90500).

Preparation of anthracene-9,10-diyl-bis[bis(4-methoxy-2,6-dimethylphenyl)methylium] bis(hexachloroantimonate) [$\mathbf{1e}^{2+}(SbCl_6^-)_2$]: To a solution of **1e** (43.0 mg, 58.0 μmol) in dry CH_2Cl_2

(1.2 mL) was added tris(4-bromophenyl)aminium hexachloroantimonate (94.6 mg, 116 µmol), and the mixture was stirred at 25 ºC for 30 min. The addition of dry ether led to precipitation of the dication salt. The precipitates were washed with dry ether five times, and collected by filtration to give **1e**$^{2+}$($SbCl_6^-$)$_2$ (397 mg) as a dark-green powder in 97% yield.
Mp: 163-164 ºC; ^{1}H NMR (400 MHz, CD_3CN): δ/ppm 7.91 (4H, brs), 7.59 (4H, brs), 7.20 (4H, s), 6.81 (4H, s), 4.08 (12H, s), 2.21 (12H, brs), 1.58 (12H, brs); ^{13}C NMR (100 MHz, CD_3CN): δ/ppm 186.97, 171.95, 154.03, 150.24, 144.22, 134.29, 130.84, 130.52, 126.88, 126.51, 121.13, 120.40, 58.05, 23.72, 23.57; IR (ATR, KBr pellet) : ν/cm^{-1} 3081, 2977, 2937, 2860, 2839, 1581, 1525, 1473, 1441, 1414, 1349, 1295, 1252, 1191, 1154, 1025, 990, 961, 929, 867, 844, 770, 752, 729, 706, 670, 605, 524, 475; LR-MS(FD) m/z (%): 742.44 (10), 741.43 (28), 740.43 ([M^{2+}+e$^-$]$^+$, 55), 739.42 (30), 738.41(21), 737.40 (8), 371.71 (8), 371.21(20), 370.71(60), 370.21(M^{2+}, bp); HR-MS (FD) Calcd. for $C_{52}H_{52}O_4$: 740.38656; Found: 740.38821; UV/Vis/NIR (CH_2Cl_2): λ_{max}/nm (ε/Lmol^{-1}cm^{-1}) 855 (21100), 650 (47100), 476 (18900), 266 (91700).

Reduction of dication salt 1c^{2+}($SbCl_6^-$)$_2$ to 1c: To a solution of **1c**$^{2+}$($SbCl_6^-$)$_2$ (30.3 mg, 22.4 µmol) in dry MeCN (1.1 mL) was added activated zinc powder (146 mg, 2.23 mmol). The mixture was stirred at 25 ºC for 30 min, and then diluted with water. The whole mixture was extracted with EtOAc five times. The combined organic layers were washed with water and brine, and dried over anhydrous Na_2SO_4. After filtration through silica gel, the solvent was concentrated under reduced pressure to give **1c** (15.1 mg) as a white solid in 98% yield.

Reduction of dication salt 1d^{2+}($SbCl_6^-$)$_2$ to 1d: To a solution of **1d**$^{2+}$($SbCl_6^-$)$_2$ (20.6 mg, 14.4 µmol) in dry MeCN (1.4 mL) was added activated zinc powder (93.0 mg, 1.42 mmol). The mixture was stirred at 25 ºC for 30 min, and then diluted with water. The whole mixture was extracted with EtOAc five times. The combined organic layers were washed with water and brine, and dried over anhydrous Na_2SO_4. After filtration through silica gel, the solvent was concentrated under reduced pressure to give **1d** (10.6 mg) as a white solid in 96% yield.

Reduction of dication salt 1e^{2+}($SbCl_6^-$)$_2$ to 1e: To a solution of **1e**$^{2+}$($SbCl_6^-$)$_2$ (13.4 mg, 9.50 µmol) in dry MeCN (1.0 mL) was added activated zinc powder (62.2 mg, 951 µmol). The mixture was stirred at 25 ºC for 30 min, and then diluted with water. The whole mixture was extracted with EtOAc five times. The combined organic layers were washed with water and brine, and dried over anhydrous Na_2SO_4. After filtration through silica gel, the solvent was concentrated under reduced pressure to give **1e** (7.0 mg) as a yellow solid in 99% yield.

X-ray analyses: A suitable crystal was selected and measured on a Rigaku XtaLAB Synergy (Cu-Kα radiation, λ = 1.54184 Å) with HyPix diffractometer. The crystal was kept at 150 K during data collection. Using Olex2,[60] the structure was solved with the SHELXT[61] structure solution program using Intrinsic Phasing and refined with the SHELXL[62] refinement package using Least Squares minimization.

*Crystal data of **1c***
Crystals were obtained by recrystallization from CH_2Cl_2/MeOH. MF: $C_{48}H_{44}O_4$, FW: 684.83, colorless plate, 0.12 × 0.05 × 0.01 mm^3, monoclinic *I*2/a, *a* = 22.0117(9) Å, *b* = 7.5538(3) Å, *c* = 25.9466(11) Å, *β* = 109.791(5)º, *V* = 4059.4(3) Å^3, *ρ* (Z = 4) = 1.121 g cm^{-3}. A total 13310 reflections were measured at *T* = 150 K. Numerical absorption correction was applied (*μ* = 0.548 mm^{-1}). The final R_1 and wR_2 values are 0.0468 (I > 2σI) and 0.1417 (all data) for 4065 reflections and 240 parameters Estimated standard deviations are 0.0018-0.002 Å for bond lengths and 0.12-0.16º for bond angles. Solvent mask procedure was used for the analysis. CCDC 2225557.

*Crystal data of **1d***
Crystals were obtained by recrystallization from $CHCl_3$/MeOH. MF: $C_{44}H_{32}Cl_4O_4$, FW: 766.49, colorless block, 0.13 × 0.10 × 0.08 mm^3, monoclinic $P2_1/c$, *a* = 13.00534(10) Å, *b* = 18.30266(16) Å, *c* = 15.93071(14) Å, *β* = 104.0340(8)º, *V* = 3678.84(6) Å^3, *ρ* (Z = 4) = 1.384 g cm^{-3}. A total 13470 reflections were measured at *T* = 150 K. Numerical absorption correction was applied (*μ* = 9.799 mm^{-1}). The final R_1 and wR_2 values are 0.0554 (I > 2σI) and 0.1471 (all data) for 13470 reflections and 529 parameters Estimated standard deviations are 0.002-0.011 Å for bond lengths and 0.17-0.5º for bond angles. CCDC 2225558.

*Crystal data of **1e***
Crystals were obtained by recrystallization from $CHCl_3$/Hexane. MF: $C_{52}H_{52}O_4$, FW: 740.93, yellow plate, 0.15 × 0.10 × 0.02 mm^3, monoclinic C2c, *a* = 48.3263(11) Å, *b* = 8.21941(16) Å, *c* = 22.3771(4) Å, *β* = 97.539(2)º, *V* = 8811.6(3) Å^3, *ρ* (Z = 8) = 1.117 g cm^{-3}. A total 13470 reflections were measured at *T* = 150 K. Numerical absorption correction was applied (*μ* = 0.538 mm^{-1}). The final R_1 and wR_2 values are 0.0528 (I > 2σI) and 0.1552 (all data) for 9069 reflections and 529 parameters Estimated standard deviations are 0.002-0.007 Å for bond lengths and 0.15-0.4º for bond angles. Solvent mask procedure was used for the analysis. CCDC 2225559.

*Crystal data of **1c**$^{2+}$($SbCl_6^-$)$_2$*
Crystals were obtained by recrystallization from dry CH_2Cl_2/ether. MF: $C_{48}H_{44}O_4Cl_{12}Sb_2$, FW: 1353.73, purple plate, 0.35 × 0.03 × 0.002 mm^3, monoclinic $P2_1/c$, *a* = 14.6910(5) Å, *b* = 10.3742(16) Å, *c* = 20.0759(8) Å, *β* = 105.698(4)º, *V* = 2945.59(19) Å^3, *ρ* (Z = 2) = 1.526 g cm^{-3}. A total 16702 reflections were measured at *T* = 150 K. Numerical absorption correction was applied (*μ* = 12.591 mm^{-1}). The final R_1 and wR_2 values are 0.0552 (I > 2σI) and 0.1679 (all data) for 5866 reflections and 387 parameters Estimated standard deviations are 0.0015-0.06 Å for bond lengths and 0.06-3.0º for bond angles. Solvent mask procedure was used for the analysis. CCDC 2225560.

*Crystal data of **1d**$^{2+}$($SbCl_6^-$)$_2$*
Crystals were obtained by recrystallization from dry CH_2Cl_2/ether. MF: $C_{44}H_{32}O_4Cl_{16}Sb_2$, FW: 1435.39, blue plate, 0.20 × 0.05 × 0.01 mm^3, triclinic *P*1bar, *a* = 9.73711(15) Å, *b* = 11.1901(2) Å, *c* = 12.8218(3) Å, *α* = 100.7375(17)º, *β* = 91.7028(16)º, *γ* = 92.4705(14)º, *V* = 1370.30(5) Å^3, *ρ* (Z = 1) = 1.739 g cm^{-3}. A total 19756 reflections were measured at *T* = 150 K. Numerical absorption correction was applied (μ = 15.327 mm^{-1}). The final R_1 and wR_2 values are 0.1130 (I > 2σI) and 0.3519 (all data) for 5578 reflections and 310 parameters Estimated standard deviations are 0.002-0.014 Å for bond lengths and 0.09-0.8º for bond angles. CCDC 2225561.

*Crystal data of **1e**$^{2+}$($SbCl_6^-$)$_2$*
Crystals were obtained by recrystallization from dry MeCN/ether. MF: $C_{52}H_{52}O_4Cl_{12}Sb_2$, FW: 1409.83, green plate, 0.20 × 0.18 × 0.03 mm^3, triclinic *P*1bar, *a* = 9.08563(8) Å, *b* = 11.33164(10) Å, *c* = 14.07306(13) Å, *α* = 95.4062(7)º, *β* = 100.5335(8)º, *γ* = 94.3919(7)º, *V* = 1411.61(2) Å^3, *ρ* (Z = 1) = 1.658 g cm^{-3}. A total 25128 reflections were measured at *T* = 100 K. Numerical absorption correction was applied (*μ* = 13.163 mm^{-1}). The final R_1 and wR_2 values are 0.0258 (I > 2σI) and 0.0730 (all data) for 5813 reflections and 326 parameters Estimated standard deviations are 0.0005-0.003 Å for bond lengths and 0.018-0.03º for bond angles. CCDC 2225562.

Acknowledgements

This work was supported by Grant-in-Aid from MEXT and JSPS (Nos. JP20H02719 and JP20K21184 to T.S., and JP21H01912 and JP21H05468 to Y.I.). T.H. is grateful for JSPS Grant-in-Aid for Research Fellow JP22J20578. Y.I. acknowledges the 2020 DIC Award in Synthetic Organic Chemistry, Japan, and the Foundation of the Promotion of Ion Engineering.

Keywords: Cations • Dyes/Pigments • NIR absorptions • X-ray analysis • *Ortho*-substitution

[1] S. Hünig, M. Kemmer, H. Wenner, I. F. Perepichka, P. Bäuerle, A. Emge, G. Gescheid, *Chem. Eur. J.* **1999**, *5*, 1969–1973.

[2] S. Hünig, M. Kemmer, H. Wenner, F. Barbosa, G. Gescheidt, I. F. Perepichka, P. Bäuerle, A. Emge, K. Peters, *Chem. Eur. J.* **2000**, *6*, 2618–2632.

[3] H. A. Shindy, *Dye. Pigment.* **2017**, *145*, 505–513.

[4] L. Hu, Z. Yan, H. Xu, *RSC Adv.* **2013**, *3*, 7667.

[5] S. Khopkar, G. Shankarling, *Dye. Pigment.* **2019**, *170*, 107645.

[6] M. Han, B. Kim, H. Lim, H. Jang, E. Kim, *Adv. Mater.* **2020**, *32*, 1905096.

[7] H. M. Kim, H. J. Lee, H. K. Lee, T. G. Hwang, J. W. Namgoong, J. M. Lee, S. Kim, J. P. Kim, *Dye. Pigment.* **2021**, *190*, 109288.

[8] Y. Liu, Z. Zhang, X. Chen, S. Xu, S. Cao, *Dye. Pigment.* **2016**, *128*, 179–189.

[9] N. Kobayashi, T. Furuyama, K. Satoh, *J. Am. Chem. Soc.* **2011**, *133*, 19642–19645.

[10] J. Fabian, H. Nakazumi, M. Matsuoka, *Chem. Rev.* **1992**, *92*, 1197–1226.

[11] K. Y. Law, *Chem. Rev.* **1993**, *93*, 449–486.

[12] L. Li, X. Dong, J. Li, J. Wei, *Dye. Pigment.* **2020**, *183*, 108756.

[13] S. Ghosh, S. Cherumukkil, C. H. Suresh, A. Ajayaghosh, *Adv. Mater.* **2017**, *29*, 1703783.

[14] H. Han, Y. J. Lee, J. Kyhm, J. S. Jeong, J. Han, M. K. Yang, K. M. Lee, Y. Choi, T. Yoon, H. Ju, S. Ahn, J. A. Lim, *Adv. Funct. Mater.* **2020**, *30*, 2006236.

[15] X. Han, X. Chen, T. Gordon, S. Holdcroft, *Macromol. Rapid Commun.* **2009**, *30*, 2089–2095.

[16] T. Okamura, T. Kitagawa, K. Koike, S. Fukuda, *J. Soc. Inf. Disp.* **2004**, *12*, 527–531.

[17] K. Yang, L. Wang, Q. Zhang, *J. Mater. Sci. Mater. Electron.* **2015**, *26*, 2222–2229.

[18] B. C. O'Regan, I. López-Duarte, M. V. Martínez-Díaz, A. Forneli, J. Albero, A. Morandeira, E. Palomares, T. Torres, J. R. Durrant, *J. Am. Chem. Soc.* **2008**, *130*, 2906–2907.

[19] N. Sekar, R. K. Raut, P. G. Umape, *Mater. Sci. Eng. B* **2010**, *168*, 259–262.

[20] M. Ince, J. Bartelmess, D. Kiessling, K. Dirian, M. V. Martínez-Díaz, T. Torres, D. M. Guldi, *Chem. Sci.* **2012**, *3*, 1472.

[21] H. Zhang, G. Wicht, C. Gretener, M. Nagel, F. Nüesch, Y. Romanyuk, J.-N. Tisserant, R. Hany, *Sol. Energy Mater. Sol. Cells* **2013**, *118*, 157–164.

[22] B. Hu, W. Zhang, J. Wu, Z. Pang, S. Zhao, Z. Lu, Y. Huang, *Dye. Pigment.* **2019**, *166*, 467–472.

[23] G. Chen, H. Sasabe, T. Igarashi, Z. Hong, J. Kido, *J. Mater. Chem. A* **2015**, *3*, 14517–14534.

[24] J. He, Y. J. Jo, X. Sun, W. Qiao, J. Ok, T. Kim, Z. Li, *Adv. Funct. Mater.* **2021**, *31*, 2008201.

[25] D. Meng, R. Zheng, Y. Zhao, E. Zhang, L. Dou, Y. Yang, *Adv. Mater.* **2022**, *34*, 2107330.

[26] J. O. Escobedo, O. Rusin, S. Lim, R. M. Strongin, *Curr. Opin. Chem. Biol.* **2010**, *14*, 64–70.

[27] S. Luo, E. Zhang, Y. Su, T. Cheng, C. Shi, *Biomaterials* **2011**, *32*, 7127–7138.

[28] A. Yuan, J. Wu, X. Tang, L. Zhao, F. Xu, Y. Hu, *J. Pharm. Sci.* **2013**, *102*, 6–28.

[29] L. Wu, Y. Sun, K. Sugimoto, Z. Luo, Y. Ishigaki, K. Pu, T. Suzuki, H.-Y. Chen, D. Ye, *J. Am. Chem. Soc.* **2018**, *140*, 16340–16352.

[30] H.-B. Cheng, Y. Li, B. Z. Tang, J. Yoon, *Chem. Soc. Rev.* **2020**, *49*, 21–31.

[31] B. Li, M. Zhao, F. Zhang, *ACS Mater. Lett.* **2020**, *2*, 905–917.

[32] L. Wu, Y. Ishigaki, Y. Hu, K. Sugimoto, W. Zeng, T. Harimoto, Y. Sun, J. He, T. Suzuki, X. Jiang, H.-Y. Chen, D. Ye, *Nat. Commun.* **2020**, *11*, 446.

[33] L. Wu, Y. Ishigaki, W. Zeng, T. Harimoto, B. Yin, Y. Chen, S. Liao, Y. Liu, Y. Sun, X. Zhang, Y. Liu, Y. Liang, P. Sun, T. Suzuki, G. Song, Q. Fan, D. Ye, *Nat. Commun.* **2021**, *12*, 6145.

[34] L. Wu, W. Zeng, Y. Ishigaki, J. Zhang, H. Bai, T. Harimoto, T. Suzuki, D. Ye, *Angew. Chem. Int. Ed.* **2022**, *61*, e202209248.

[35] P. Monk, R. Mortimer, D. Rosseinsky, *Electrochromism and Electrochromic Devices*, Cambridge University Press, Cambridge, **2007**.

[36] D. R. Rosseinsky, P. M. S. Monk, R. J. Mortimer, *Electrochromic Materials and Devices*, Wiley-VCH, Weinheim, Germany, **2013**.

[37] S. Mujawar, P. Patil, *Electrochromism in Pristine and Doped Niobium Oxide Thin Films: Spray Pyrolytic Synthesis of Niobium Oxide Thin Films for Smart Window Application*, LAP LAMBERT Academic Publishing, **2016**.

[38] W. Zhang, H. Li, E. Hopmann, A. Y. Elezzabi, *Nanophotonics* **2020**, *10*, 825–850.

[39] Z. Wang, X. Wang, S. Cong, J. Chen, H. Sun, Z. Chen, G. Song, F. Geng, Q. Chen, Z. Zhao, *Nat. Commun.* **2020**, *11*, 302.

[40] B. Li, J. Dang, Q. Zhuang, Z. Lv, *Chem. – An Asian J.* **2022**, *17*, e202200022.

[41] T. Suzuki, Y. Sakano, Y. Tokimizu, Y. Miura, R. Katoono, K. Fujiwara, N. Yoshioka, N. Fujii, H. Ohno, *Chem. Asian J.* **2014**, *9*, 1841–1846.

[42] C. Zhu, X. Ji, D. You, T. L. Chen, A. U. Mu, K. P. Barker, L. M. Klivansky, Y. Liu, L. Fang, *J. Am. Chem. Soc.* **2018**, *140*, 18173–18182.

[43] D. T. Christiansen, A. L. Tomlinson, J. R. Reynolds, *J. Am. Chem. Soc.* **2019**, *141*, 3859–3862.

[44] P. W. Antoni, T. Bruckhoff, M. M. Hansmann, *J. Am. Chem. Soc.* **2019**, *141*, 9701–9711.

[45] Y. Ishigaki, T. Harimoto, K. Sugimoto, L. Wu, W. Zeng, D. Ye, T. Suzuki, *Chem. – An Asian J.* **2020**, *15*, 1147–1155.

[46] P. Rietsch, S. Sobottka, K. Hoffmann, A. A. Popov, P. Hildebrandt, B. Sarkar, U. Resch‐Genger, S. Eigler, *Chem. – A Eur. J.* **2020**, *26*, 17361–17365.

[47] R. Rausch, M. I. S. Röhr, D. Schmidt, I. Krummenacher, H. Braunschweig, F. Würthner, *Chem. Sci.* **2021**, *12*, 793–802.

[48] Y. Ishigaki, T. Harimoto, K. Sugawara, T. Suzuki, *J. Am. Chem. Soc.* **2021**, *143*, 3306–3311.

[49] B. Sk, M. Sarkar, K. Singh, A. Sengupta, A. Patra, *Chem. Commun.* **2021**, *57*, 13590–13593.

[50] P. W. Antoni, C. Golz, M. M. Hansmann, *Angew. Chem. Int. Ed.* **2022**, *61*, e202203064.

[51] Y. Ishigaki, M. Takata, T. Shimajiri, L. Wu, W. Zeng, D. Ye, T. Suzuki, *Chem. – A Eur. J.* **2022**, *28*, e202202457.

[52] Y. Ishigaki, K. Sugawara, M. Yoshida, M. Kato, T. Suzuki, *Bull. Chem. Soc. Jpn.* **2019**, *92*, 1211–1217.

[53] Y. Ishigaki, K. Sugawara, T. Tadokoro, Y. Hayashi, T. Harimoto, T. Suzuki, *Chem. Commun.* **2021**, *57*, 7201–7214.

[54] R. Neidlein, M. Winter, *Synthesis (Stuttg).* **1998**, *1998*, 1362–1366.

[55] Y. Sakano, R. Katoono, K. Fujiwara, T. Suzuki, *Chem. Lett.* **2014**, *43*, 1143–1145.

[56] M. J. Frisch, G. W. Trucks, H. B. Schlegel, G. E. Scuseria, M. A. Robb, J. R. Cheeseman, G. Scalmani, V. Barone, G. A. Petersson, X. Nakatsuji, H.; Li, M. Caricato, A. V. Marenich, J. Bloino, B. G. Janesko, R. Gomperts, B. Mennucci, H. P. Hratchian, J. V. Ortiz, A. F. Izmaylov, J. L. Sonnenberg, D. Williams-Young, F. Ding, F. Lipparini, F. Egidi, J. Goings, B. Peng, A. Petrone, T. Henderson, D. Ranasinghe, V. G. Zakrzewski, J. Gao, N. Rega, G. Zheng, W. Liang, M. Hada, M. Ehara, K. Toyota, R. Fukuda, J. Hasegawa, M. Ishida, T. Nakajima, Y. Honda, O. Kitao, H. Nakai, T. Vreven, K. Throssell, J. A. J. Montgomery, J. E. Peralta, F. Ogliaro, M. J. Bearpark, J. J. Heyd, E. N. Brothers, K. N. Kudin, V. N. Staroverov, T. A. Keith, R. Kobayashi, J. Normand, K. Raghavachari, A. P. Rendell, J. C. Burant, S. S. Iyengar, J. Tomasi, M. Cossi, J. M. Millam, M. Klene, C. Adamo, R. Cammi, J. W. Ochterski, R. L. Martin, K. Morokuma, O. Farkas, J. B. Foresman, D. J. Fox, *Gaussian 16, Revision B.01*, Gaussian, Inc., Wallingford CT, **2016**.

[57] M. R. Talipov, M. M. Hossain, A. Boddeda, K. Thakur, R. Rathore, *Org. Biomol. Chem.* **2016**, *14*, 2961–2968.

[58] L. V. Ivanova, T. S. Navale, D. Wang, S. Lindeman, M. V. Ivanov, R. Rathore, *Chem. Commun.* **2018**, *54*, 5851–5854.

[59] F. C. Görth, M. Rucker, M. Eckhardt, R. Brückner, *Eur. J. Org. Chem.* **2000**, 2605–2611.

[60] O. V. Dolomanov, L. J. Bourhis, R. J. Gildea, J. A. K. Howard, H. Puschmann, *J. Appl. Crystallogr.* **2009**, *42*, 339–341.

[61] G. M. Sheldrick, *Acta Crystallogr. Sect. A Found. Adv.* **2015**, *71*, 3–8.

[62] G. M. Sheldrick, *Acta Crystallogr. Sect. C Struct. Chem.* **2015**, *71*, 3–8.

Entry for the Table of Contents

Insert graphic for Table of Contents here.

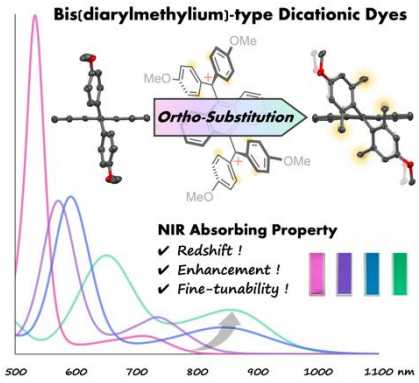

An *ortho*-substitution strategy is key for controlling both steric and electronic effects of bis(diarylmethylium)-type dicationic dyes. It was proven to be an effective strategy for fine-tuning of their LUMO levels, resulting in the red-shift and enhancement of NIR-absorbing abilities (see picture).

Institute and/or researcher Twitter usernames: Takashi Harimoto (@ZhangBen_dyrex), Yusuke Ishigaki (@ysk_isgk), and Laboratory (@Yuuichi_Hokudai)